Effects of Black Carbon Aerosols on the Indian Monsoon

GERALD A. MEEHL, JULIE M. ARBLASTER,* AND WILLIAM D. COLLINS

National Center for Atmospheric Research,+ Boulder, Colorado

(Manuscript received 17 November 2006, in final form 25 May 2007)

ABSTRACT

A six-member ensemble of twentieth-century simulations with changes to only time-evolving global distributions of black carbon aerosols in a global coupled climate model is analyzed to study the effects of black carbon (BC) aerosols on the Indian monsoon. The BC aerosols act to increase lower-tropospheric heating over South Asia and reduce the amount of solar radiation reaching the surface during the dry season, as noted in previous studies. The increased meridional tropospheric temperature gradient in the premonsoon months of March–April–May (MAM), particularly between the elevated heat source of the Tibetan Plateau and areas to the south, contributes to enhanced precipitation over India in those months. With the onset of the monsoon, the reduced surface temperatures in the Bay of Bengal, Arabian Sea, and over India that extend to the Himalayas act to reduce monsoon rainfall over India itself, with some small increases over the Tibetan Plateau. Precipitation over China generally decreases due to the BC aerosol effects. There is a weakened latitudinal SST gradient resulting from BC aerosols in the model simulations as seen in the observations, and this is present in the multiple-forcings experiments with the Community Climate System Model, version 3 (CCSM3), which includes natural and anthropogenic forcings (including BC aerosols). The BC aerosols and consequent weakened latitudinal SST gradient in those experiments are associated with increased precipitation during MAM in northern India and over the Tibetan Plateau, with some decreased precipitation over southwest India, the Bay of Bengal, Burma, Thailand, and Malaysia, as seen in observations. During the summer monsoon season, the model experiments show that BC aerosols have likely contributed to observed decreasing precipitation trends over parts of India, Bangladesh, Burma, and Thailand. Analysis of single ensemble members from the multiple-forcings experiment suggests that the observed increasing precipitation trends over southern China appear to be associated with natural variability connected to surface temperature changes in the northwest Pacific.

1. Introduction

Modeling studies have shown that that black carbon (BC) aerosols can affect the monsoons of Asia (e.g., Menon et al. 2002; Ramanathan et al. 2005). These BC aerosols make up a significant part of what has been called the atmospheric brown cloud (ABC) over Asia (Ramanathan and Crutzen 2003). The black carbon considered in this study represents the soot produced by fossil fuel combustion and biomass burning (Collins et al. 2002). These BC aerosols both absorb and reflect incoming solar radiation, thus heating the lower troposphere and cooling the surface (Meywerk and Ramanathan 1999). The effects of the ABC on longwave radiation are contributed primarily by natural aerosols and are not appreciable for anthropogenic BC (Ramanathan et al. 2001). Lau et al. (2006) have pointed out that such ABC aerosols can combine with naturally occurring dust loading over the Tibetan Plateau to accentuate the elevated heat source during the premonsoon months, thus enhancing the meridional temperature gradient and contributing to increased rainfall over India during the premonsoon and summer monsoon seasons. However, their experiments were done with a model that had fixed sea surface temperatures (SSTs). Ramanathan et al. (2005), using a global coupled cli-

* Additional affiliation: Bureau of Meteorology Research Centre, Melbourne, Victoria, Australia.

+ The National Center for Atmospheric Research is sponsored by the National Science Foundation.

Corresponding author address: Gerald A. Meehl, National Center for Atmospheric Research, P.O. Box 3000, Boulder, CO 80307.
E-mail: meehl@ncar.ucar.edu

DOI: 10.1175/2007JCLI1777.1

mate model with an interactive ocean and specifying BC aerosols only over the Indian region, showed that BC aerosols can indeed increase premonsoon rainfall, but actually can reduce Indian summer monsoon rainfall in part due to the effects of ocean coupling and consequent cooler SSTs in the northern Indian Ocean. Additionally, the effects of BC aerosols may extend beyond areas where their concentrations are greatest, perhaps effecting precipitation and SSTs over the tropical Pacific (Wang 2007).

Chung et al. (2002) used an atmospheric model with fixed SSTs and specified ABC aerosols (only over South Asia) for the dry months (November–May) to show that their effect was to decrease solar radiation at the surface with consequent surface cooling, but to absorb radiation in the lower troposphere, producing heating there with an enhancement of the meridional temperature gradient and stronger premonsoon rainfall (their experiment was not applicable to the summer monsoon season). Menon et al. (2002) also used a climate model with fixed SSTs, and showed a mixture of both increased and decreased precipitation over India during the summer monsoon season as a result of relatively dark ABC aerosols (specified only over the Asian region), representing a high proportion of BC, with decreased precipitation over the northern Indian Ocean and northern China, and increased precipitation over South China. Chung and Ramanathan (2006) performed sensitivity experiments to show that the observed weakening of the meridional SST gradient between the Bay of Bengal and Arabian Sea and the Indian Ocean to the south in the second half of the twentieth century (possibly resulting from the increase of ABC aerosols with a high BC content) could have contributed to observed decreases in monsoon rainfall over India. Though the net global effects of BC aerosols do not significantly influence the attribution of temperature change resulting from greenhouse gases (GHGs), significant regional cooling over India, parts of China, and West Africa was noted in experiments with an atmospheric model coupled to a nondynamic slab ocean that included BC aerosols (Jones et al. 2005). If only the effects of the recent observed increase of greenhouse gases were affecting the Indian monsoon, the monsoon season rainfall should have been increasing (e.g., Meehl et al. 2000a). The fact that Indian monsoon precipitation has been observed to be decreasing suggests that aerosols may have been playing a role, as argued by the studies cited above.

For twentieth-century experiments with a global coupled climate model, the Community Climate System Model, version 3 (CCSM3; model documented by Collins et al. 2006), included combinations of natural and anthropogenic forcings, as well as globally and seasonally varying distributions of both reflecting and absorbing BC aerosols scaled in time over the twentieth century by global human population increase (Meehl et al. 2006a). In previous experiments with another model [the Parallel Climate Model (PCM)], Meehl et al. (2004) documented climate system responses to the individual anthropogenic (GHGs, the direct effect of sulfate aerosols, ozone) and natural (volcanoes, solar) forcings, and their various combinations. These experiments showed that the observed globally averaged warming in the second half of the twentieth century could only have occurred with a substantial contribution from anthropogenic forcings. For the CCSM3 twentieth-century experiments (Meehl et al. 2006b), there were comparable anthropogenic and natural forcings as in the PCM, but BC aerosols were also included (along with prescribed seasonally and spatially varying distributions of mineral dust and sea salt, but with no trend in time). Subsequently, twentieth-century simulations were performed where only BC aerosols were changed (because they were specified in the multiple-forcings simulations). Here we compare these experiments with a control run to determine the BC aerosol role in the response of the multiple-forcings experiments.

Therefore, the purpose of the present paper is to determine the effects on the climate system of including BC aerosols in the simulations of twentieth-century climate. Though the BC time- and space-varying distributions are global in extent in CCSM3, we focus here on the Asian monsoon region because effects of BC aerosols have been shown to likely be significant in that region (as noted above).

2. Description of model and experiments

The CCSM3, which is used in this paper, is described by Collins et al. (2006). We analyze twentieth-century simulations from the T85 version of CCSM3, with grid points in the atmosphere roughly every 1.4° latitude and longitude, and 26 levels in the vertical, with the top two model hybrid-level midpoints at 3.54 and 7.39 hPa. The ocean is a version of the Parallel Ocean Program (POP) with a nominal latitude–longitude resolution of 1° (1/2° in the equatorial tropics) and 40 levels in the vertical, and Gent–McWilliams and K-profile parameterization (KPP) mixing. The land surface model is the Community Land Model (CLM), and the elastic–viscous–plastic (EVP) dynamic and thermodynamic sea ice component is the Community Sea Ice Model version 4 (CSIM4; all described in Collins et al. 2006). No flux adjustments are used in the CCSM3. The CCSM3 simu-

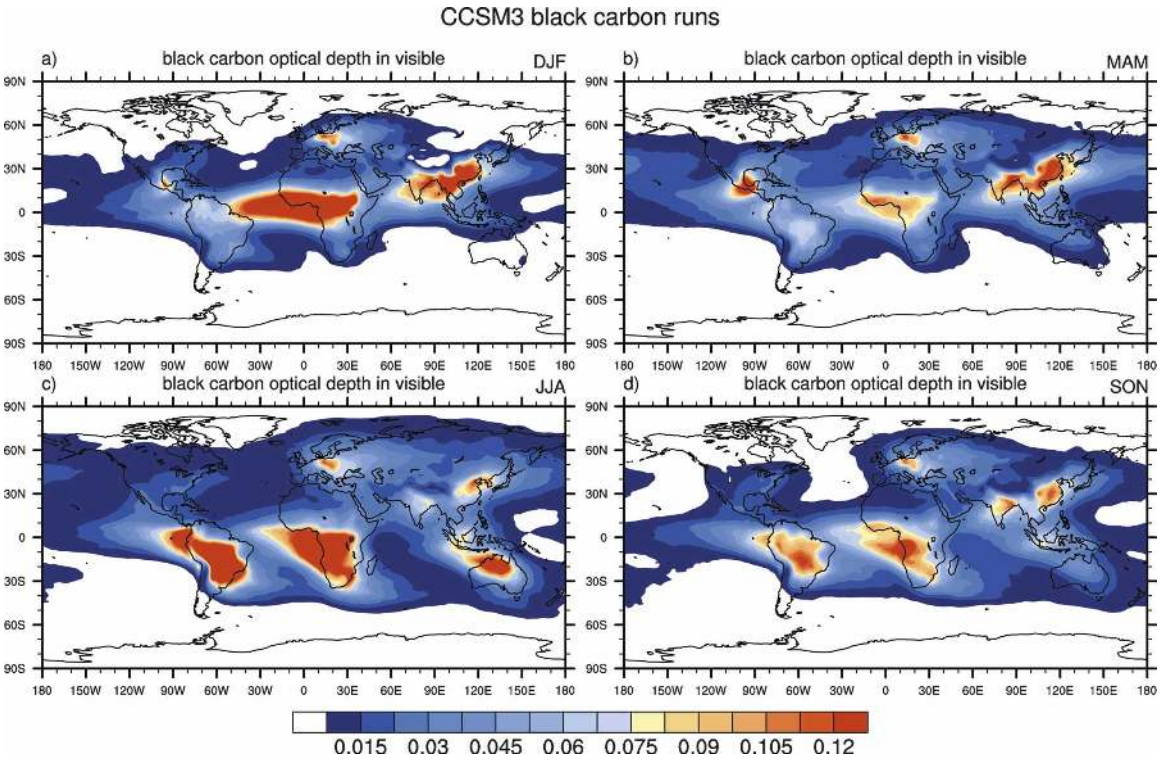

FIG. 1. Distributions of black carbon optical depth for 1999 by season: (a) DJF, (b) MAM, (c) JJA, and (d) September–November (SON). This pattern was scaled back in time based on globally averaged human population.

lation represents many of the regional and seasonal aspects of the South Asian monsoon (Meehl et al. 2006b).

The CCSM3 was run for a preindustrial (1870) control run that was used as an initial state for the twentieth-century simulations (Meehl et al. 2006a). A five-member ensemble of CCSM3 twentieth-century multiple-forcing simulations is analyzed here. The twentieth-century simulations were started from different times in the 1870 control run and were separated by 20 yr, with the first ensemble member branching from the control run at year 360. The natural (volcanoes and solar) and anthropogenic (GHGs, sulfate direct, black carbon, and ozone) forcings are described in Meehl et al. (2006a). The CCSM3 twentieth-century simulations include time- and space-varying global distributions of BC aerosols, as noted above. A present-day distribution was generated from a three-dimensional assimilation model described by Collins (2001) and Rasch et al. (2001). To summarize briefly, the aerosol assimilation system consists of the Model for Atmospheric Chemistry and Transport (MATCH) and an assimilation of satellite retrievals of aerosol optical depth. MATCH version 4 is integrated using the National Centers for Environmental Predication–National Center for Atmospheric Research (NCEP–NCAR) reanalysis at T63 resolution. The satellite estimates of aerosol optical depth are from the National Oceanic and Atmospheric Administration (NOAA) Pathfinder II dataset. The sources of black carbon are based upon climatological inventories of aerosols produced by fossil fuel combustion and biomass burning (Collins et al. 2002). The aerosols are treated as external mixtures. For the ABC, the shortwave aerosol function changes by less than 10% if the aerosol particles are treated as homogeneous internal mixtures of the various aerosol species (Ramanathan et al. 2001). An ensemble of aerosol models, including MATCH, simulates the absorption optical depth and imaginary index of refraction of the ABC in eastern Asia with reasonable fidelity relative to the Aerosol Robotic Network (AERONET) surface observations (Kinne et al. 2006). The vertical profiles of the ABC produced by MATCH over the Pacific are in good agreement with aircraft observations (Clarke et al. 2001), although the model does not reproduce the frequency of elevated aerosol plumes over the Indian Ocean (Rasch et al. 2001).

The BC aerosols are a combination of black and organic carbon that both absorb and reflect solar radiation. The indirect effects of BC aerosols on cloud albedo and cloud lifetime are not included, although the semidirect effects on cloud amount are treated (Ackerman et al. 2000). Also included in the multiple-

forcings twentieth-century climate simulations were climatological monthly present-day fixed-concentration (i.e., no trend in time) global distributions of mineral dust and sea salt, also generated from the three-dimensional assimilation (Collins 2001; Rasch et al. 2001).

Subsequently, a six-member ensemble of twentieth-century climate simulations was performed with the CCSM3, where only the BC aerosols changed over the course of the twentieth century. These simulations branched from starting points in the 1870 control run separated by 20 yr, and the pattern of BC aerosols (the pattern derived from present-day emissions) was increased as a function of global population from 1870 values to the 1999 distributions, which are shown for the four seasons in Fig. 1. There are significant geographic differences in the BC distributions with season. Note the large contrasts between December–February (DJF) and June–August (JJA) over tropical South America, Africa, south Asia, Indonesia, and Australia. Corresponding rainfall differences generally show decreased rainfall over regions with large BC concentrations, in particular the West African monsoon in JJA (not shown). There are interesting seasonal differences in BC over south Asia (Fig. 1), with large values in the dry season [DJF and March–May (MAM) seasons, in particular], and a sharp drop during the summer monsoon season (JJA). These seasonal changes will turn out to be important in the analyses to follow. For the model simulations to be analyzed here, because all other forcings were held at their 1870 values, the difference between the BC simulations and the 1870 control run quantifies the effects of BC alone on the climate system. Differences, where applicable, will be computed as ensemble averages for the period of 1980–99 (for BC aerosol experiments minus comparable periods in the 1870 control run).

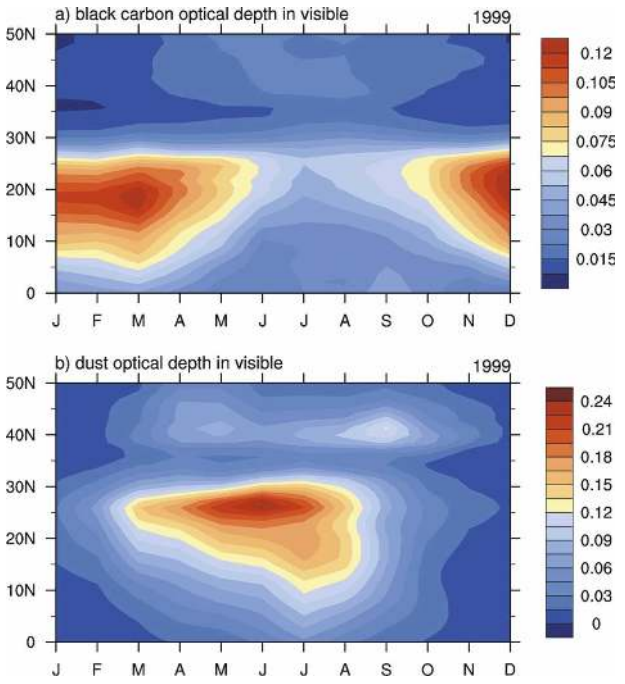

FIG. 2. (a) Seasonal cycle of BC optical depth in the visible divided by the portion of time the column is lit (because zeros are recorded for nighttime values) for 1999 (see note on scaling to other years in caption to Fig. 1), averaged over the Indian sector from 70° to 100°E; (b) same as (a), but for mineral dust, which remains constant throughout the experiments; (c) same as (a), but for sulfate aerosols from a representative ensemble member.

3. Effects of BC aerosols on the Indian monsoon

As noted above, there are interesting seasonal variations of BC over the south Asian region. Figure 2a shows this seasonal cycle of BC aerosols as a function of month for 1999, averaged over the Indian longitude sector from 70° to 100°E. Maximum values occur throughout the dry season from October to May in the latitudes from about 10° to 25°N, with minimum values during the rainy monsoon season of June–September (the BC is rained out during the monsoon). In contrast, the dust aerosol seasonal cycle is almost opposite to that of BC (Fig. 2b), with maximum loading from March to August at somewhat higher latitudes (about 20°–30°N). Recall in these experiments that the dust loadings in Fig. 1b are constant throughout the experiments, but the concentrations of BC aerosols increase (with the same pattern) as a function of population through the course of the twentieth century. The sulfate aerosol seasonal cycle is similar to dust, with maximum values near 20°N during the monsoon season (not shown). Radiative forcing from sulfate aerosols influences South Asia throughout the year (e.g., Meehl et al. 2000b). The possible effects of sulfate aerosols versus carbon aerosols will be discussed later.

The interplay between the seasonal cycles of BC and dust has been pointed out, for example, by Lau et al. (2006). They noted the importance of black carbon in the premonsoon months in altering the vertical and meridional profiles of heating. For the present experiment, Fig. 3 shows the shortwave heating rate differences for the black carbon experiments minus the control run. Note that stippling in this figure and the ones to follow indicates areas where the ensemble mean signal divided by the interensemble standard deviation exceeds 1.0, and is a measure of consistency of model response to facilitate interpretation of physical significance (e.g., Cubasch et al. 2001). The effect of black carbon is to warm the lower troposphere below about 700 hPa south of the Tibetan Plateau during March, April, and May.

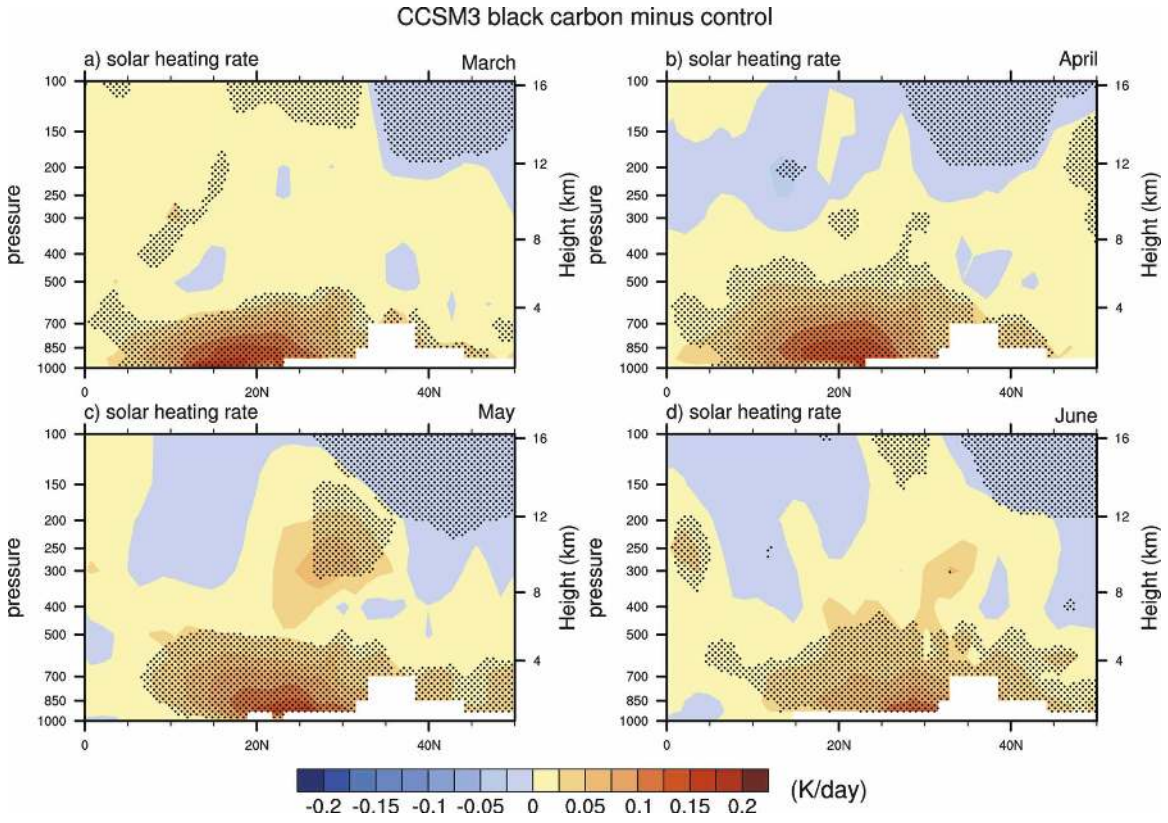

FIG. 3. Latitude–height sections, averaged over the Indian sector from 70° to 100°E, for solar heating rate (K day^{-1}) resulting from BC aerosols, differences are computed for the six-member ensemble mean BC aerosol-only experiments (1980–99) minus the comparable time period in the 1870 preindustrial control run for (a) March, (b) April, (c) May, and (d) June. Stippling indicates areas where the ensemble mean signal divided by the interensemble standard deviation exceeds 1.0. Pressure level data blocked by topography are denoted by white areas that extend farther south over India as the monsoon low pressure trough becomes established in May and June.

By June, when the black carbon aerosol loading decreases (Fig. 2a), so does the corresponding heating. With this heating in the lower troposphere, net solar radiation at the surface decreases. Ensemble area averages over the region of 5°–25°N, 70°–90°E, land points only for the Indian region, show a decrease of net solar radiation at the surface for the MAM premonsoon season of -6.5 W m^{-2} (with a decrease in net solar at the top of the atmosphere of only -1.0 W m^{-2}, indicating that about 85% of the change in solar radiation seen at the surface is due to absorption by the BC aerosols). This reduction of net solar radiation at the surface is about half the observed decrease from 1960 to 2000 from surface stations over India (Ramanathan et al. 2005, their Fig. 2a). Though part of the observed dimming could also be due to sulfate aerosols, this implies that the black carbon forcing could be underestimated in part due to the lack of indirect effects of black carbon aerosols in the model. This will be revisited in the discussion of the interpretation of the multiple-forcings experiments in comparison to observations later. If ocean points are included as well from the 5°–25°N, 60°–95°E region, the change in net solar at the top of the atmosphere for the MAM season is -0.5 W m^{-2} (with a total change in net radiative flux at the top of the atmosphere of -0.8 W m^{-2}), while the reduction of solar radiation at the surface is -4.1 W m^{-2}. The longwave heating rates (not shown) change with the alterations in vertical temperature profiles, but these changes result from the shortwave effects of the ABC, as discussed in the introduction.

Consequently, surface temperatures decrease over the Indian region south of the Tibetan Plateau in the premonsoon months (Fig. 4), with the largest decreases consistent across the ensemble members (denoted in the figure by stippling) of about 1°C during May (Fig. 4c). The consistent decreases of surface temperature extend over the Arabian Sea and Bay of Bengal, with smaller amplitude. Thus, the dynamic coupling of the ocean and atmosphere plays a key role in changing surface temperatures over land and ocean regions.

Meanwhile, to the north over the elevated heat

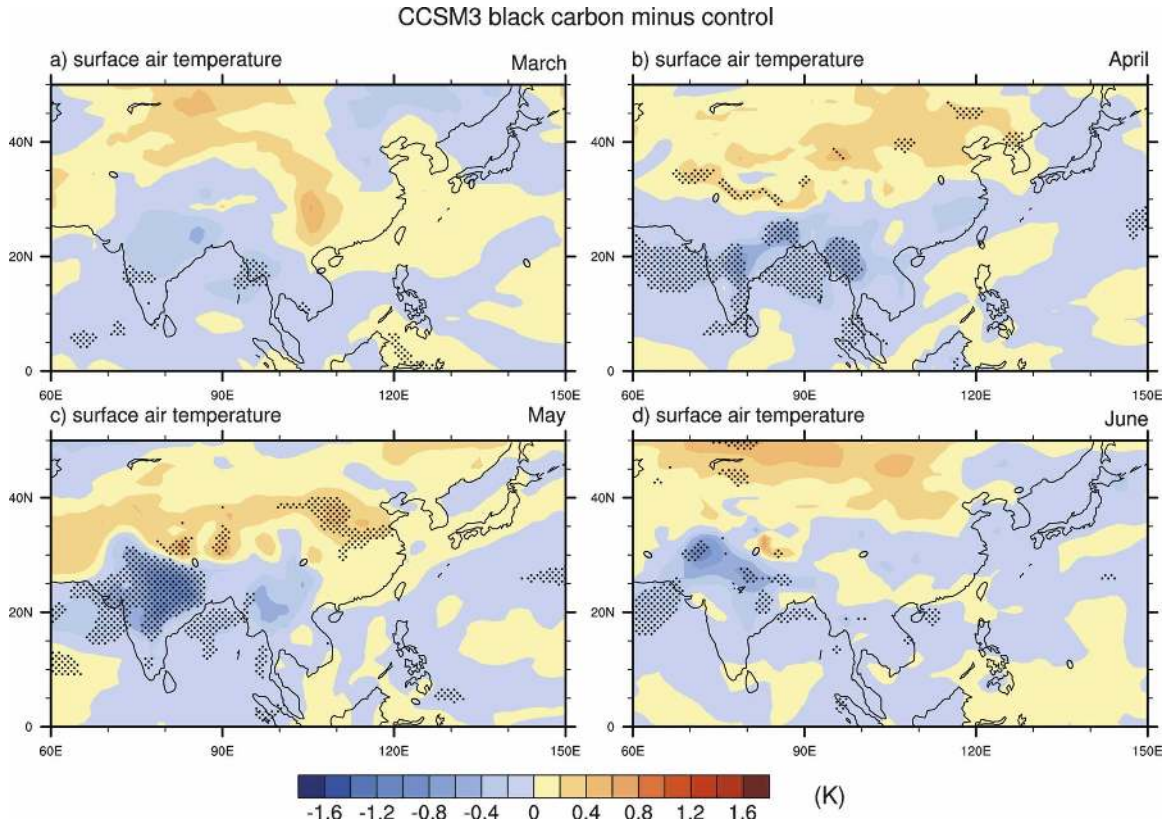

FIG. 4. Surface air temperature differences resulting from BC aerosols, differences computed for the six-member ensemble mean BC aerosol-only experiments (1980–99) minus the comparable time period in the control for (a) March, (b) April, (c) May, and (d) June. Stippling indicates areas where the ensemble mean signal divided by the interensemble standard deviation exceeds 1.0.

source of the Tibetan Plateau, there are increases of temperature in each of the premonsoon months approaching 0.5°C (Fig. 4). Lau et al. (2006) referred to an "elevated heat pump," such that the effects of the shortwave heating from black carbon, combined with the elevated topography north of India, results in the advection of the warmer air northward and upward over the Tibetan Plateau. This produces increased temperatures through a significant depth of the troposphere over the Tibetan Plateau in the premonsoon months of March, April, and May (Fig. 5), as well as at the surface (Fig. 4). This has the additional effect of reducing snow depth over the Tibetan Plateau by about 10%–20% (not shown), which also contributes to warmer surface temperatures and the enhanced meridional temperature gradient that strengthens the monsoon (e.g., Meehl 1994).

The increase of the tropospheric meridional temperature gradient, associated with the consistent cooling over South Asia and warming over the elevated heat source of the Tibetan Plateau region during MAM (Fig. 6a), produces increases of rainfall up to about 0.4 mm day^{-1} (roughly 10%) over India during the MAM premonsoon season (Fig. 6b). This is associated with higher sea level pressure (SLP) over South Asia (Fig. 6c) and corresponding anomalous southerlies over much of India that carry moisture from the Indian Ocean over the Indian land area, and warmer air in the lower troposphere, up and over the Tibetan Plateau (Fig. 6d). Meanwhile, the increased SLP over India and parts of Burma and Thailand is associated with anomalous northerly component offshore surface winds over China (Fig. 6d) that cut off the moisture source from the South China Sea, with consequent decreases of precipitation over China during MAM (Fig. 6b) resulting from the BC aerosols.

As the BC aerosols are reduced during the monsoon months (Fig. 1a), their influence also decreases. However, conditions that were set up in MAM influence the subsequent outcome of the Indian summer monsoon. As the anomalous meridional temperature gradient shifts north in June at the surface, with the greatest anomalous warming near 45°N while northern India is consistently cool (Fig. 4d), the anomalous meridional temperature gradient in the troposphere also is dominated by cooling over nearly the entire Indian sector,

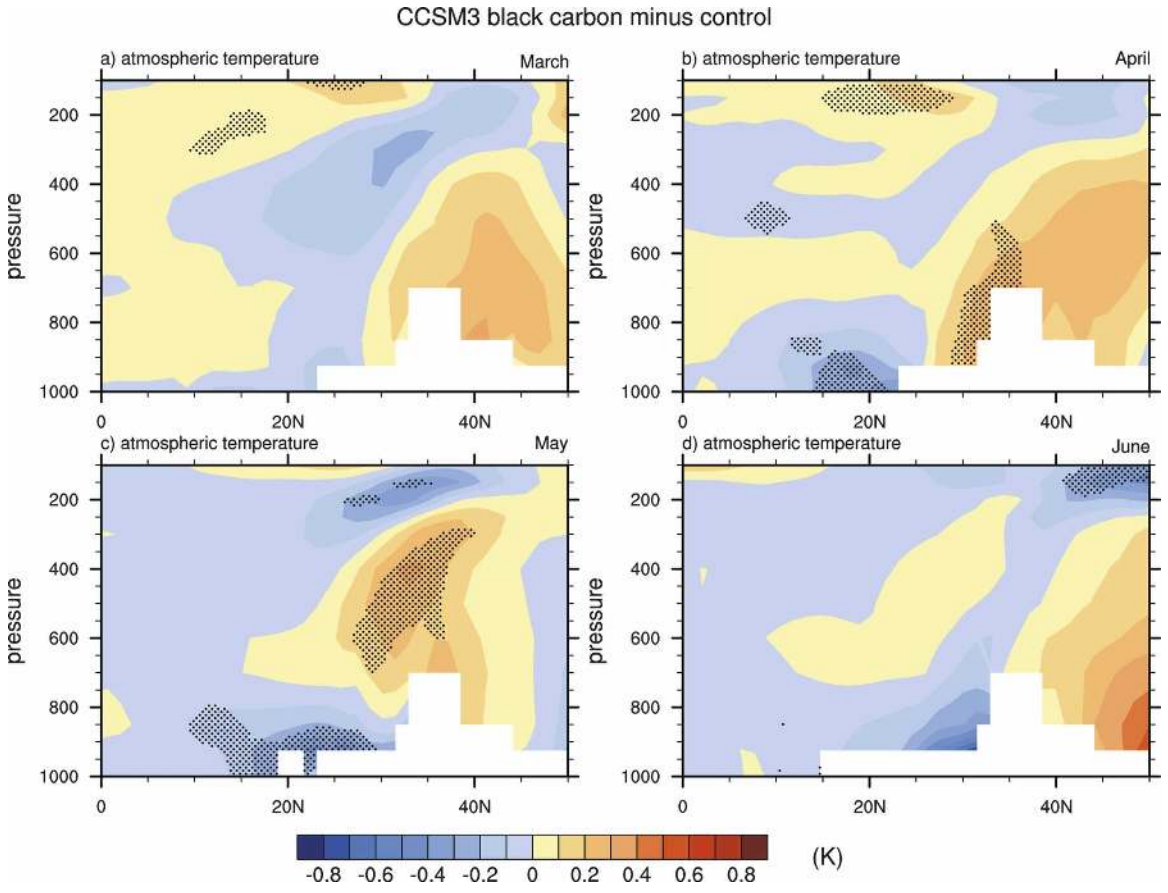

FIG. 5. Latitude–height sections, averaged over the Indian sector from 70° to 100°E for the temperature response resulting from BC aerosols, differences are computed for the six-member ensemble mean BC aerosol-only experiments (1980–99) minus the comparable time period in the control for (a) March, (b) April, (c) May, and (d) June. Stippling indicates areas where the ensemble mean signal divided by the interensemble standard deviation exceeds 1.0.

with deep anomalous heating well to the north near 45°N (Fig. 5d). Therefore, for the JJA monsoon season, much of South Asia is anomalously cool, including much of the Arabian Sea and Bay of Bengal (Fig. 7a), with consequent decreases of rainfall over much of India, the Bay of Bengal, and the Arabian Sea, and only small increases well to the north near 35°N, and to the south near the ITCZ over the Indian Ocean near 5°N (Fig. 7b). This pattern, induced by the presence of BC aerosols, is similar to "break" monsoon conditions over India when the monsoon trough and associated rainfall shift northward over the foothills of the Himalayas with a consequent reduction of monsoon rainfall over India (Ding and Sikka 2006). This type of condition was noted to be associated with the effects of BC aerosols and weakened north Indian Ocean SST gradients (Chung and Ramanathan 2006). That is, the SST decreases in the Arabian Sea and Bay of Bengal (Fig. 7a) contribute to precipitation decreases there (Fig. 7b), while the SST increases near 5°N (Fig. 7a) are conducive to increases of precipitation there (Fig. 7b). Similar effects of Indian Ocean SSTs on Indian region monsoon rainfall were noted in sensitivity experiments by Meehl and Arblaster (2002, see their Fig. 8).

Rainfall is decreased over most of China, as well due to BC aerosols, particularly north China, while it is increased over parts of Thailand, Laos, and Vietnam, and baiu rainfall over Japan is increased (Fig. 7b). The decrease of rainfall over India is associated with positive SLP anomalies (Fig. 7c) and an anomalous anticyclonic circulation over the western coast of India (Fig. 7d), while anomalous cyclonic circulations over the South China Sea and east China Sea (Fig. 7d) contribute to the decreased mei-yu rainfall over southern China and the increased baiu rainfall over Japan [Fig. 7b; for more description of these circulation characteristics associated with variations in these regional rainfall regimes see, e.g., Ding and Sikka (2006)]. Therefore, the effects of BC aerosols are to increase premonsoon rainfall over India and decrease it during the monsoon season, with

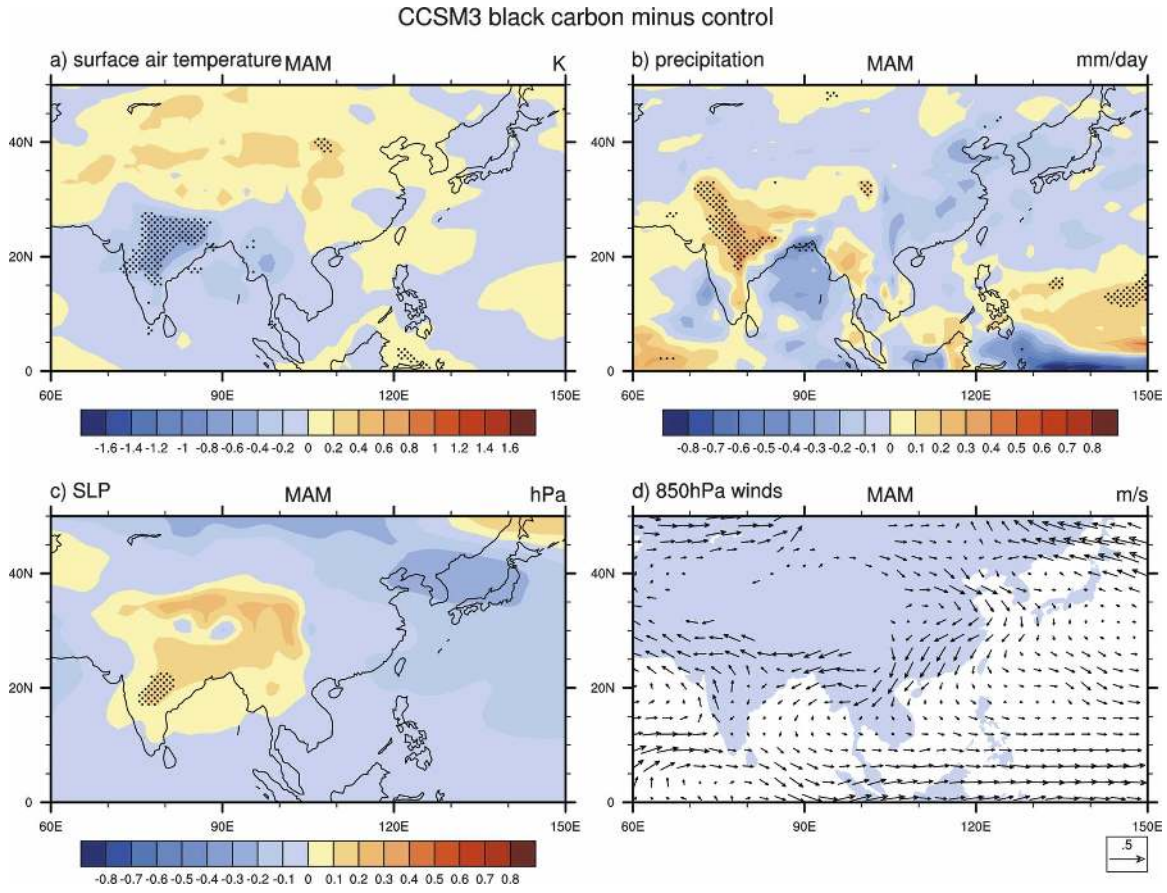

FIG. 6. Effects of BC aerosols during the premonsoon season of MAM on (a) surface air temperature (°C), (b) precipitation (mm day^{-1}), (c) SLP (hPa), and (d) 850-hPa winds (scaling vector of 0.5 m s^{-1} at lower right). Stippling indicates areas where the ensemble mean signal divided by the interensemble standard deviation exceeds 1.0.

season-averaged break monsoon conditions associated with cooler SSTs in the Arabian Sea and Bay of Bengal and warmer SSTs just to the south, thus weakening the latitudinal SST gradient.

To illustrate this weakening of the latitudinal SST gradient, Fig. 8a shows zonally averaged SST differences, for BC aerosol experiments (1980–99) minus the 1870 control, for the Indian sector of 60°–100°E for June. As noted above, the weakening latitudinal SST gradient as a consequence of the BC aerosols is characterized by negative differences that are greater in magnitude north of about 10°N, with the biggest decreases of nearly −0.15°C near 20°N, and small positive differences between the equator and 5°N. To see how these effects of BC aerosols are manifested in the multiple-forcings experiment, Fig. 8b shows a similar plot for those experiments for the same month and sector, 1980–99 minus 1930–50. We choose these periods for this difference because we will be examining trends from 1950 to 1999, so we want to find the difference of a recent 20-yr period (1980–99) minus the 20 yr just prior to 1950. Though SSTs increase at all latitudes, the increases are greatest near about 5°N, with values approaching +0.4°C, with the lowest amplitude increases of about +0.25°C near 20°N. The observations [from the Hadley Centre Sea Ice and SST dataset (HadISST) dataset as documented by Rayner et al. (2003)] from this time period (Fig. 8b) show a greater decrease of SST gradient, with the largest values above +0.4°C near 5°N, decreasing to about +0.1°C at 20°N. Both the model and observations indicate a weakening latitudinal SST gradient. To provide an indication of the contribution of BC aerosols to the weakening of latitudinal SST gradient in the multiple-forcings experiment, Fig. 8b also includes values for the difference of the multiple-forcings SSTs minus the BC aerosol experiment, with zonal means calculated in the same way as the multiple-forcings experiment [assuming linear additivity to a first order, e.g., Meehl et al. (2004)]. As expected from Fig. 7, the effect of the BC aerosols is to

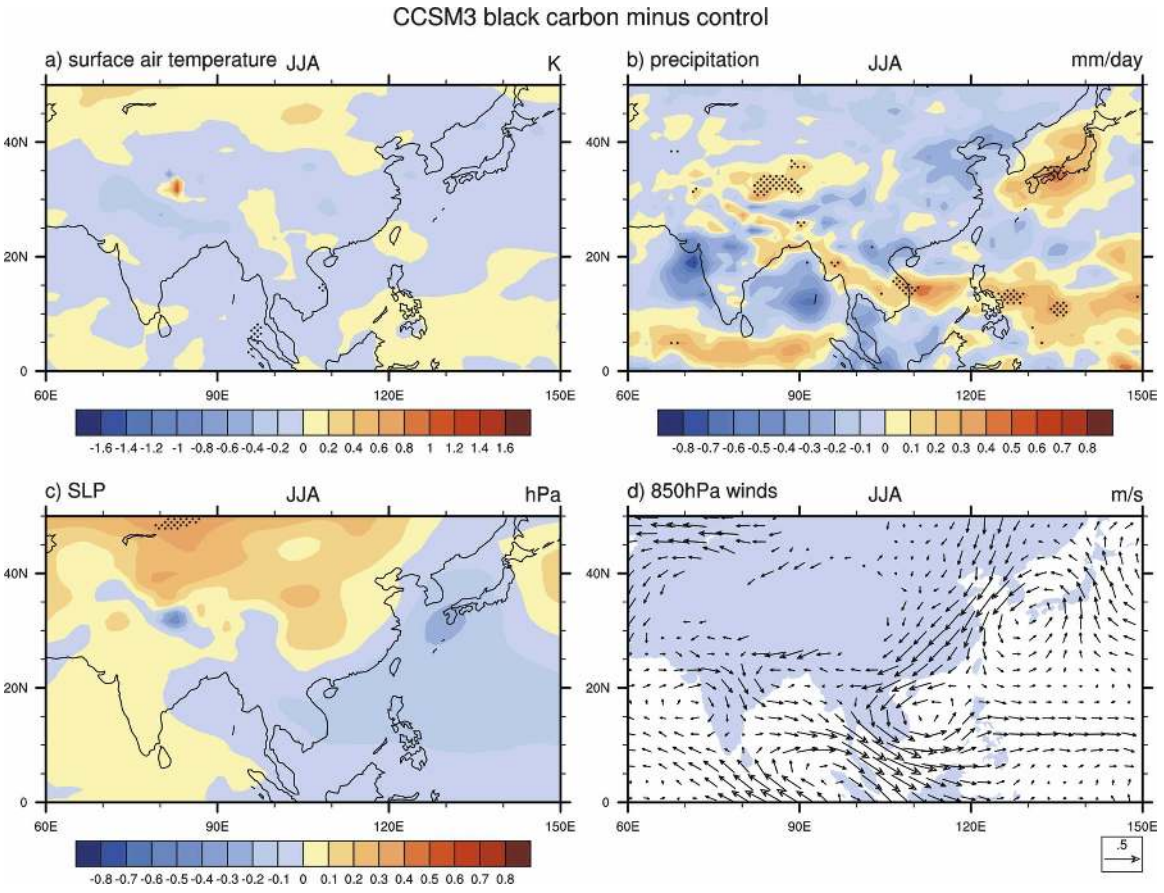

FIG. 7. Same as Fig. 6, but for the monsoon season of JJA.

decrease SSTs, particularly in the northern Indian Ocean, resulting from the cooler surface temperatures there, with the reduction being nearly 0.1°C.

The contributions of these changes in SST gradient are evident in Fig. 9, which shows the trend in the premonsoon season (MAM) precipitation from 1950 to 1999 for the observations (Fig. 9a) compared to the five-member ensemble mean of the CCSM3 multiple-forcings experiments (Fig. 9b). Both the observations and the model results show decreased precipitation over southwest India, much of Burma, Thailand, Malaysia, Laos, Vietnam, and China, with increasing trends in northeast India, and over the areas of the Tibetan Plateau to the north (note the different color scales for the two panels; the observed trends are about twice the magnitude of the model).

For the monsoon season itself [June–September (JJAS), see Fig. 10], comparing the multiple-forcings results (Fig. 10b) to the BC aerosol experiment precipitation changes (Fig. 7b), the consistent increase of precipitation just south of India, stretching across the Indian Ocean near 5°–10°N at the same latitude where there is the largest warming of SSTs (Fig. 8b), is comparable to the band of increased precipitation near 5°N from BC aerosols (Fig. 7b). Similarly, increased rainfall over the Tibetan Plateau, Laos, Vietnam, and Japan was also seen in the BC aerosol experiments (Fig. 7b). The decreases of rainfall over parts of India and the Bay of Bengal, southern China, and Taiwan are associated with the decreased precipitation over those regions from BC aerosols (Fig. 7b). In comparing the multiple-forcings precipitation trends (Fig. 10b) to the observed trends for the monsoon season (Fig. 10a), though the decreasing precipitation trends over India are greater in the observations (area-averaged precipitation difference over the area of 15°–30°N, 75°–95°E of -0.81 mm day^{-1}) compared to the model (area-averaged precipitation difference over that same area of -0.04 mm day^{-1}), the patterns are similar over parts of that region, with increasing trends over the Tibetan Plateau, and decreasing trends over Bangladesh, Burma, and Thailand.

Examination of the individual ensemble members for the multiple-forcings experiment shows comparable patterns of precipitation trends to the ensemble mean in Fig. 10b, but with varying amplitudes. The greatest

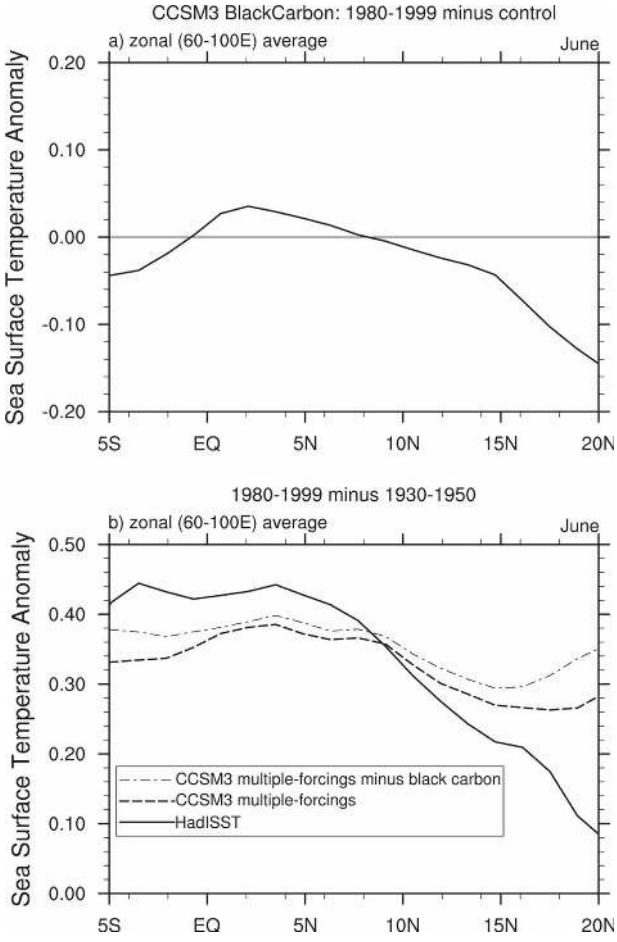

FIG. 8. (a) Zonal mean SST differences (°C) for the 60°–100°E sector ensemble mean BC aerosol experiments (1980–99) minus the control for June; (b) same as (a), but for the CCSM3 multiple-forcings experiments (solid) of 1980–99 minus 1930–50, HADISST observations (dashed), and CCSM3 multiple-forcings minus black carbon only (dash–dot).

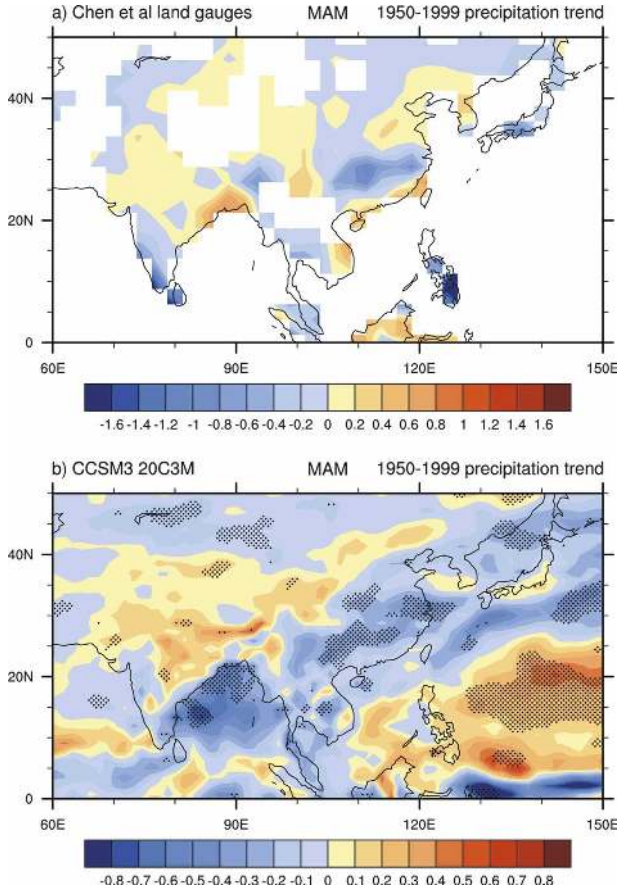

FIG. 9. Precipitation trends [(mm day^{-1}) (50 yr)$^{-1}$] for the premonsoon season (MAM) of 1950–99 for (a) observed data derived from rain gauges (Chen et al. 2002) and (b) five-member ensemble mean for the CCSM3 multiple-forcings experiments, where stippling indicates areas where the ensemble mean signal divided by the interensemble standard deviation exceeds 1.0. Note that the color scale is a factor of 2 smaller in (a) compared to (b).

decrease of area-averaged precipitation for the Indian region is -0.31 mm day^{-1}, which is still less than half the amplitude of the observed trends in that region. This suggests the possibility that the aerosol forcing is not large enough in the model, and that the inclusion of aerosol indirect effects could bring the model into closer agreement with the observations.

Additionally, there is disagreement in sign over southern China between the observed and the multiple-forcings model precipitation trends for the summer monsoon season (Fig. 10). This suggests that either the changes there are not related to changes in forcing and could perhaps be linked to inherent decadal time-scale variability (the ensemble mean results from the model represent the forced response because inherent variability is averaged out for the most part), or there are model errors that do not allow a reasonable simulation of observed precipitation trends over China (though the pattern of observed precipitation trends over much of China in MAM in Fig. 9a is well simulated by the model ensemble mean in Fig. 9b).

To further explore the possible role of natural internal variability in the model results in Fig. 10, Fig. 11 compares the observed surface temperature trends (Smith and Reynolds 2005; Fig. 11a) to the multiple-forcings ensemble mean (Fig. 11b) for the JJAS season. Both show relatively less warming trends over northern India; but over China the model ensemble mean (Fig. 11b) shows a greater warming trend over southern China compared to northern China, while the observations (Fig. 11a) show the opposite, consistent with the different model and observed precipitation trends in Fig. 10 in that region. The other notable difference between the model and observed temperature trends in Fig. 11 is that the observations (Fig. 11a) show a cooling

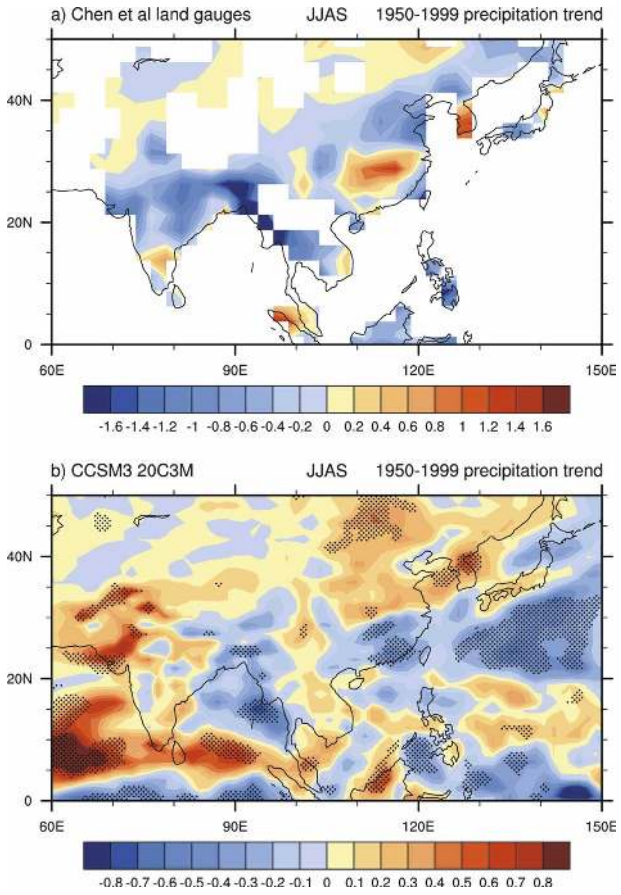

FIG. 10. Precipitation trends [mm day^{-1} (50 yr)$^{-1}$] for the monsoon season (JJAS) of 1950–99 for (a) the observed data derived from rain gauges (Chen et al. 2002) and (b) five-member ensemble mean for the CCSM3 multiple-forcings experiments, where stippling indicates areas where the ensemble mean signal divided by the interensemble standard deviation exceeds 1.0. Note that the color scale is a factor of 2 smaller in (a) compared to (b).

trend over the ocean east and southeast of Japan, while the model ensemble mean shows relatively uniform warming over this region, with somewhat greater warming near Japan than to the south. The assumption is that a multimember ensemble mean averages out any internal variability and leaves only the signal of the forced response. If that is the case, the implication of the observed negative temperature trends in the Pacific (Fig. 11a) is that they are a manifestation of internal variability, and that these SST trends affect the surface temperature trends over China to the west, where minimum warming stretches from the Pacific near Japan, across Korea, to southern China.

Because the observations are a single realization of climate variability and change, we examined the trends in the individual multiple-forcings members from CCSM3 and found one that had some cooling trends over the Pacific near Japan that extended to southern China (Fig. 11d), similar to that observed in Fig. 11a. Because the ensemble mean in Fig. 11b does not show any such cooling trends, the assumption is that inherent natural variability in the ensemble member in Fig. 11d produced the cooling trends over the northwestern Pacific extending over southern China. The associated precipitation trends from that ensemble member are shown in Fig. 11c, and mostly show increases of precipitation over southern China in contrast to the decreases of precipitation in the multimember ensemble mean in Fig. 10b. The single ensemble member in Fig. 11c with northwest Pacific temperature trends more closely resembling those in the observations also produces precipitation trends over China more like the observed precipitation trends in Fig. 10a. This suggests that at least part of the observed temperature and precipitation trends over China could have been due to inherent natural variability in the northwest Pacific, as evidenced by the results from the single ensemble member compared to the multimember ensemble mean.

Another possibility is that effects from sulfate aerosols may be contributing to some of the multiple-forcings temperature and precipitation signals in the premonsoon and monsoon seasons. There are no sulfate-only experiments from the CCSM3, but such experiments were run with the PCM (Meehl et al. 2004). To provide an indication of what the contributions could be from sulfate aerosols in CCSM3, we show surface air temperature and precipitation differences for MAM (Figs. 12a,b, respectively), and for JJA (Figs. 12c,d, respectively) for a four-member sulfates-only ensemble mean from the PCM. Both seasons mostly show decreases of surface temperature associated with the reflection of incoming solar radiation from the sulfate aerosols (sulfates in this prescription have no absorbing properties in either PCM or CCSM3). Consequently, there are decreases of precipitation in both MAM and JJA. However, there are marked differences in the response to sulfates in PCM and BC aerosols in CCSM3. As noted in Figs. 3–6, the absorption of solar radiation in the lower troposphere by the BC aerosols in MAM helps to produce cooling over India and warming to the north over the Tibetan Plateau (Fig. 6a). The resulting enhanced meridional temperature gradient contributes to increased precipitation over India from BC aerosols in MAM (Fig. 6c). In contrast, the purely reflective properties of the sulfate aerosols produce cooling over all of South Asia, in addition to consequent *decreases* of precipitation in MAM (Figs. 12a,b). Thus, the increases of precipitation over India in MAM in both the observations and the multiple-forcings experiments (Fig. 9) are likely due to the increases of BC aerosols over the

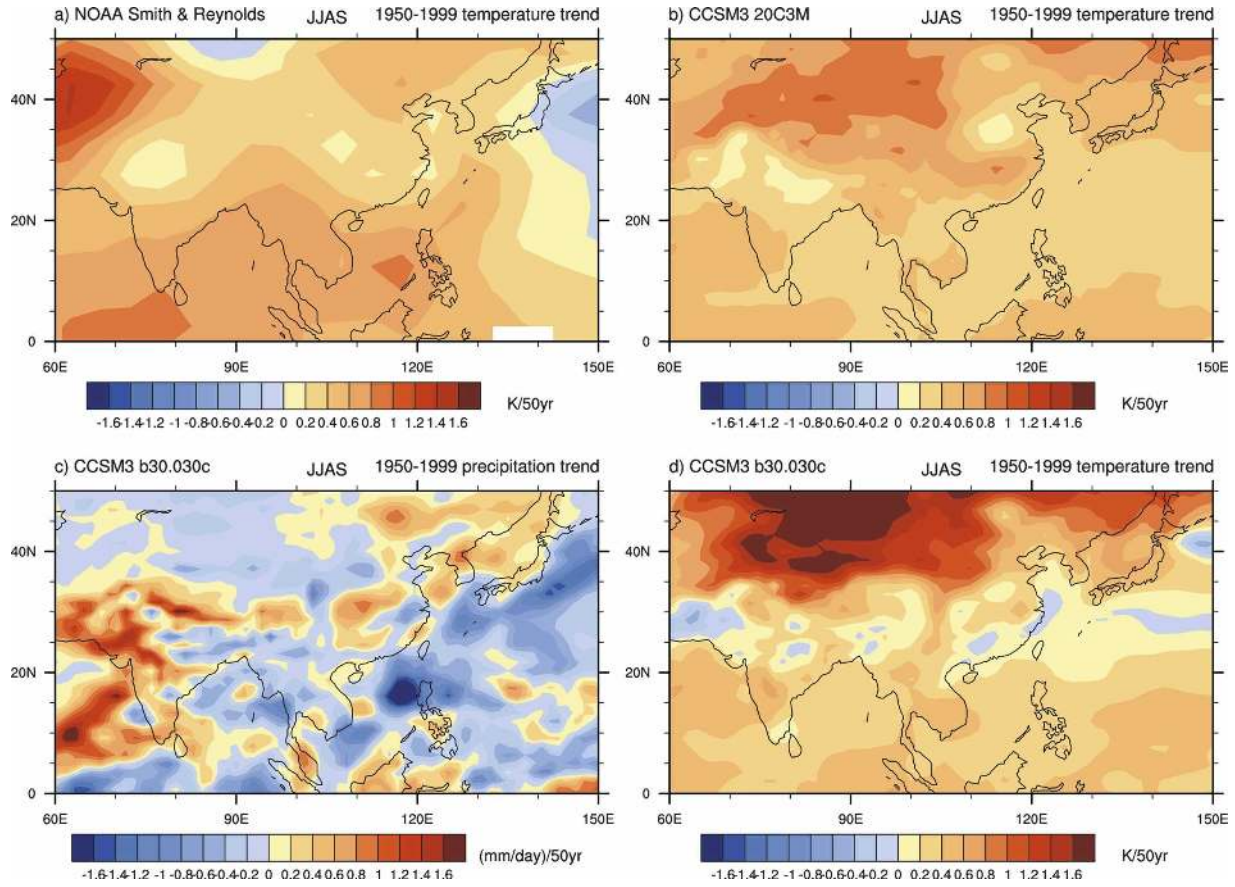

FIG. 11. (a) Observed surface temperature trends [°C (50 yr)$^{-1}$] for the monsoon season (JJAS) of 1950–99 (Smith and Reynolds 2005). (b) Same as (a), but for the five-member ensemble mean for the CCSM3 multiple-forcings experiments; (c) same as (b), but for precipitation from a single ensemble member; and (d) same as (b), but for a single ensemble member. No stippling has been applied in this figure.

second half of the twentieth century. However, sulfate aerosols could have contributed in part to the decreases of monsoon rainfall over the Indian region in the summer monsoon season in the observations and multiple-forcings experiments (Fig. 10), because BC and sulfate aerosols both are acting to decrease rainfall in the Indian region during the monsoon season and are being opposed by the tendency to enhance monsoon rainfall resulting from increases of GHGs (e.g., Meehl and Arblaster 2003).

4. Conclusions

To study the effects of black carbon aerosols on the Indian monsoon, a six-member ensemble of twentieth-century simulations is performed with only BC aerosols varying, while all other natural and anthropogenic forcings are fixed at their preindustrial values. Differences of the BC simulations minus the 1870 preindustrial control run highlight the effects of BC aerosols on the Indian monsoon regime. The radiative effects of BC aerosols are most dramatic during the dry season over South Asia, in particular for the premonsoon months of March–April–May. Surface temperatures cool over most of India, the Bay of Bengal, and the Arabian Sea because of the decreased solar radiation at the surface caused by the absorption and reflection of solar radiation by the BC aerosols. The warmer air from the effects of the shortwave heating in the lower troposphere is advected northward and manifested by warming over the elevated heat source of the Tibetan Plateau, thus producing an anomalously strengthened meridional temperature gradient through most of the depth of the troposphere during MAM. Consequently, there is anomalous inflow from the Indian Ocean to the south, and enhanced rainfall over most of India during the premonsoon season of MAM. However, as the BC aerosol concentrations decrease during the monsoon season, the anomalous elevated heat source and meridional temperature gradient decreases. This, in com-

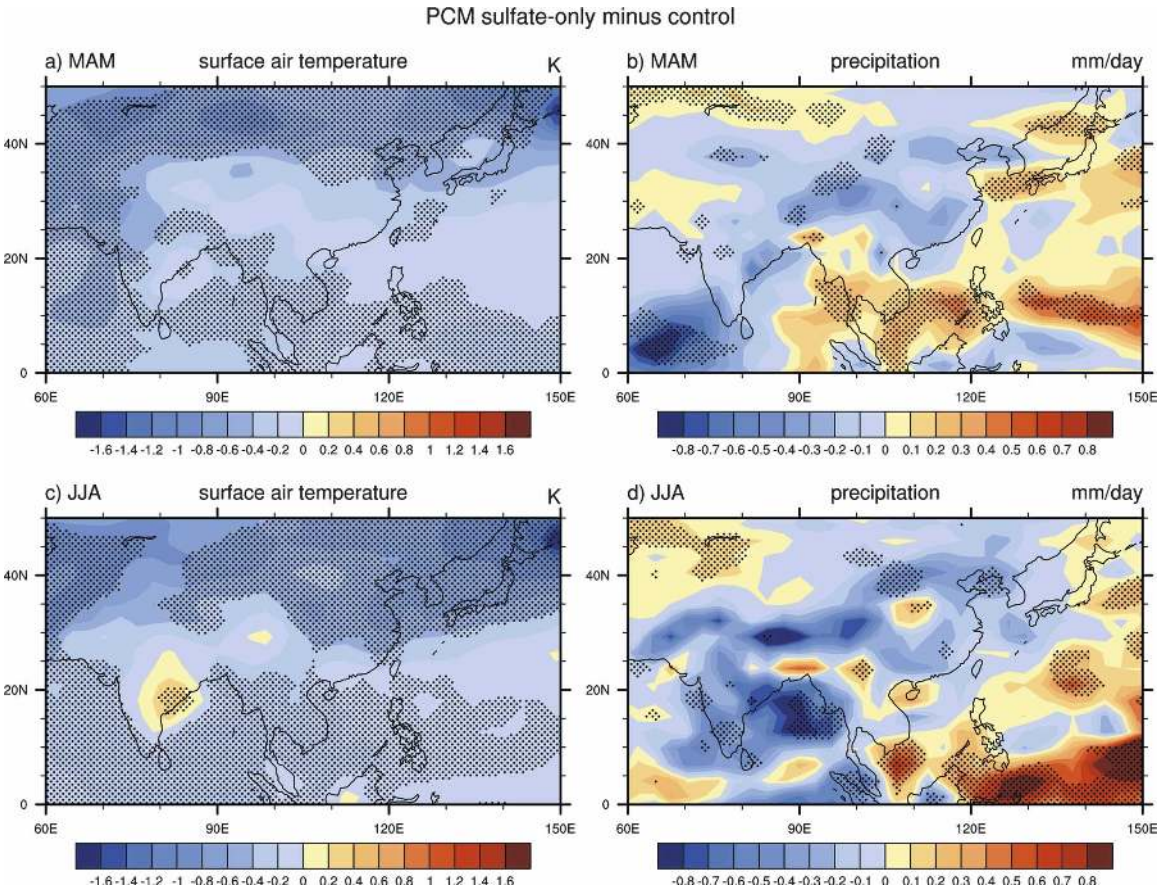

FIG. 12. From the PCM the effects of sulfate aerosols during the premonsoon season of MAM on (a) surface air temperature (°C) and (b) precipitation (mm day^{-1}) are shown; (c) same as (a), but for JJA, and (d) same as (b), but for JJA. Stippling indicates areas where the ensemble mean signal divided by the interensemble standard deviation exceeds 1.0.

bination with the anomalously cool SSTs in the Arabian Sea and Bay of Bengal left from the effects of the BC aerosol effects in MAM, produce reduced rainfall over much of India, the Arabian Sea, and the Bay of Bengal during the monsoon season of JJA.

The effects of the BC aerosols are also felt over China, with weakened mei-yu rainfall during JJA that extends over northern China. Meanwhile, parts of Southeast Asia experience increased rainfall, and there is enhanced baiu rainfall over Japan. The role of the BC aerosols in precipitation trends over the second half of the twentieth century in multiple-forcings experiments with CCSM3 (with natural and anthropogenic forcings, including BC aerosols) compared to observations shows similar patterns in MAM and JJAS (though the decreases in precipitation over India are less in the ensemble mean multiple-forcings experiments), suggesting that the BC aerosols play an important role in observed precipitation trends over much of South Asia. However, there is little agreement in the model and observed precipitation trends over China during JJAS (suggesting either model errors or other processes could be playing a role in that region). An examination of surface temperature trends from the multiple-forcings ensemble mean and observations indicate that inherent natural variability over the northwest Pacific, extending to southern China, could have influenced the observed precipitation trends that show increases over southern China. One member of the multiple-forcings experiment shows similar negative surface temperature trends over the northwest Pacific extending over southern China, and consequent precipitation trends that show an increasing precipitation trend more in line with the observations. This suggests that inherent natural variability may have played a larger role than the forcing from BC aerosols over southern China in the second half of the twentieth century.

These experiments point to the regional importance of BC aerosols for rainfall patterns over much of Asia, and in the Indian monsoon region in particular, and rely in part on changes to SSTs in the Arabian Sea and Bay of Bengal during MAM that extend to the summer

monsoon season to contribute to the decreases of rainfall over parts of India due to BC aerosols.

Acknowledgments. NOAA Merged Air Land and SST Anomalies data provided by NOAA/OAR/ESRL PSD, Boulder, Colorado, from their Web site at http://www.cdc.noaa.gov/. HadISST data were obtained from http://www.metoffice.gov.uk/hadobs. Portions of this research were supported by the Office of Science (BER), U.S. Department of Energy Cooperative Agreement DE-FC02-97ER62402, and the National Science Foundation.

REFERENCES

Ackerman, A. S., O. B. Toon, D. E. Stevens, A. J. Heymsfield, V. Ramanathan, and E. J. Welton, 2000: Reduction of tropical cloudiness by soot. *Science,* **288,** 1042–1047.

Chen, M., P. Xie, J. E. Janowiak, and P. A. Arkin, 2002: Global land precipitation: A 50-yr monthly analysis based on gauge observations. *J. Hydrometeor.,* **3,** 249–266.

Chung, C. E., and V. Ramanathan, 2006: Weakening of North Indian SST gradients and the monsoon rainfall in India and the Sahel. *J. Climate,* **19,** 2036–2045.

——, ——, and J. T. Kiehl, 2002: Effects of the South Asian absorbing haze on the northeast monsoon and surface–air heat exchange. *J. Climate,* **15,** 2462–2476.

Clarke, A., W. D. Collins, P. J. Rasch, V. Kapustin, K. Moore, and S. Howell, 2001: Pollution transport on global scales: Measurements and model predictions. *J. Geophys. Res.,* **106,** 32 555–32 570.

Collins, W. D., 2001: Parameterization of generalized cloud overlap for radiative calculations in general circulation models. *J. Atmos. Sci.,* **58,** 3224–3242.

——, P. J. Rasch, B. E. Eaton, D. W. Fillmore, J. T. Kiehl, T. C. Beck, and C. S. Zender, 2002: Simulation of aerosol distributions and radiative forcing for INDOEX: Regional climate impacts. *J. Geophys. Res.,* **107,** 8028, doi:10.1029/2000JD000032.

——, and Coauthors, 2006: The Community Climate System Model version 3 (CCSM3). *J. Climate,* **19,** 2122–2143.

Cubasch, U., and Coauthors, 2001: Projections of future climate change. *Climate Change 2001: The Scientific Basis,* J. T. Houghton et al., Eds., Cambridge University Press, 525–582.

Ding, Y., and D. R. Sikka, 2006: Synoptic systems and weather. *The Asian Monsoon,* B. Wang, Ed., Springer-Verlag, 131–201.

Jones, G. S., A. Jones, D. L. Roberts, P. A. Stott, and K. D. Williams, 2005: Sensitivity of global-scale climate change attribution results to inclusion of fossil fuel black carbon aerosol. *Geophys. Res. Lett.,* **32,** L14701, doi:10.1029/2005GL023370.

Kinne, S., and Coauthors, 2006: An AeroCom initial assessment—Optical properties in aerosol component modules of global models. *Atmos. Chem. Phys.,* **6,** 1815–1834.

Lau, K. M., M. K. Kim, and K. M. Kim, 2006: Asian summer monsoon anomalies induced by aerosol direct forcing: The role of the Tibetan Plateau. *Climate Dyn.,* **26,** 855–864.

Meehl, G. A., 1994: Coupled land–ocean–atmosphere processes and south Asian monsoon variability. *Science,* **266,** 263–267.

——, and J. M. Arblaster, 2002: GCM sensitivity experiments for the Indian monsoon and tropospheric biennial oscillation transition conditions. *J. Climate,* **15,** 923–944.

——, and ——, 2003: Mechanisms of projected future changes in south Asian monsoon precipitation. *Climate Dyn.,* **21,** 659–675.

——, W. D. Collins, B. Boville, J. T. Kiehl, T. M. L. Wigley, and J. M. Arblaster, 2000a: Response of the NCAR Climate System Model to increased CO_2 and the role of physical processes. *J. Climate,* **13,** 1879–1898.

——, W. M. Washington, J. M. Arblaster, T. W. Bettge, and W. G. Strand Jr., 2000b: Anthropogenic forcing and decadal climate variability in sensitivity experiments of twentieth- and twenty-first-century climate. *J. Climate,* **13,** 3728–3744.

——, ——, C. Amman, J. M. Arblaster, T. M. L. Wigley, and C. Tebaldi, 2004: Combinations of natural and anthropogenic forcings in twentieth-century climate. *J. Climate,* **17,** 3721–3727.

——, and Coauthors, 2006a: Climate change projections for twenty-first century and climate change commitment in the CCSM3. *J. Climate,* **19,** 2597–2616.

——, J. M. Arblaster, D. Lawrence, A. Seth, E. K. Schneider, B. P. Kirtman, and D. Min, 2006b: Monsoon regimes in the CCSM3. *J. Climate,* **19,** 2482–2495.

Menon, S., J. Hansen, L. Nazarenko, and Y. Luo, 2002: Climate effects of black carbon aerosols in China and India. *Science,* **297,** 2250–2253.

Meywerk, J., and V. Ramanathan, 1999: Observations of the spectral clear-sky aerosol forcing over the tropical Indian Ocean. *J. Geophys. Res.,* **104,** 24 359–24 370.

Ramanathan, V., and P. J. Crutzen, 2003: New directions: Atmospheric brown "clouds." *Atmos. Environ.,* **37,** 4033–4035.

——, and Coauthors, 2001: The Indian Ocean experiment: An integrated assessment of the climate forcing and effects of the great Indo-Asian haze. *J. Geophys. Res.,* **106,** 28 371–28 398.

——, and Coauthors, 2005: Atmospheric brown clouds: Impacts on South Asian climate and hydrological cycle. *Proc. Natl. Acad. Sci. USA,* **102,** 5326–5333.

Rasch, P. J., W. D. Collins, and B. E. Eaton, 2001: Understanding the Indian Ocean Experiment (INDOEX) aerosol distributions with an aerosol assimilation. *J. Geophys. Res.,* **106,** 7337–7356.

Rayner, N. A., D. E. Parker, E. B. Horton, C. K. Folland, L. V. Alexander, D. P. Rowell, E. C. Kent, and A. Kaplan, 2003: Global analyses of sea surface temperature, sea ice, and night marine air temperature since the late nineteenth century. *J. Geophys. Res.,* **108,** 4407, doi:10.1029/2002JD002670.

Smith, T. M., and R. W. Reynolds, 2005: A global merged land–air–sea surface temperature reconstruction based on historical observations (1880–1997). *J. Climate,* **18,** 2021–2036.

Wang, C., 2007: Impact of direct radiative forcing of black carbon aerosols on tropical convective precipitation. *Geophys. Res. Lett.,* **34,** L05709, doi:10.1029/2006GL028416.